

# Correlated photon dynamics in dissipative Rydberg media

Emil Zeuthen,<sup>1,2,\*</sup> Michael J. Gullans,<sup>3</sup> Mohammad F. Maghrebi,<sup>3,4</sup> and Alexey V. Gorshkov<sup>3</sup>

<sup>1</sup>*Niels Bohr Institute, University of Copenhagen, DK-2100 Copenhagen, Denmark*

<sup>2</sup>*Institute for Theoretical Physics and Institute for Gravitational Physics (Albert Einstein Institute), Leibniz Universität Hannover, Callinstraße 38, 30167 Hannover, Germany*

<sup>3</sup>*Joint Quantum Institute and Joint Center for Quantum Information and Computer Science, National Institute of Standards and Technology and University of Maryland, College Park, Maryland 20742, USA*

<sup>4</sup>*Department of Physics and Astronomy, Michigan State University, East Lansing, Michigan 48824, USA*

Rydberg blockade physics in optically dense atomic media under the conditions of electromagnetically induced transparency (EIT) leads to strong dissipative interactions between single photons. We introduce a new approach to analyzing this challenging many-body problem in the limit of large optical depth per blockade radius. In our approach, we separate the single-polariton EIT physics from Rydberg-Rydberg interactions in a serialized manner while using a hard-sphere model for the latter, thus capturing the dualistic particle-wave nature of light as it manifests itself in dissipative Rydberg-EIT media. Using this approach, we analyze the saturation behavior of the transmission through one-dimensional Rydberg-EIT media in the regime of non-perturbative dissipative interactions relevant to current experiments. Our model is able to capture the many-body dynamics of bright, coherent pulses through these strongly interacting media. We compare our model with available experimental data in this regime and find good agreement. We also analyze a scheme for generating regular trains of single photons from continuous-wave input and derive its scaling behavior in the presence of imperfect single-photon EIT.

In optically dense atomic media, strong non-linear dissipative [1–6] and dispersive [7–9] inter-photon interactions at the single-quantum level can be engineered via interactions of hybrid atom-photon excitations called Rydberg polaritons [10, 11], propagating due to Electromagnetically Induced Transparency (EIT) [12]. Such photon-photon interactions can implement quantum gates between a pair of photons [13–15]; experimental realizations in this area include single-photon phase gates [16] and transistors [17, 18]. These interactions between photons can also lead to the generation of anti-bunched [4, 19] and other non-classical [6, 20–26] states of light.

The rich physics of dissipative Rydberg-EIT media and their potential as building blocks in quantum information science make urgent the challenge to understand the underlying quantum many-body dynamics. Whereas the few-photon theory has been established [4], a tractable approach for analyzing the high-intensity sector of interest to ongoing experiments [4, 27] has thus far not been available. In this Letter, we overcome these shortcomings by constructing a model for the many-body dynamics of one-dimensional dissipative Rydberg-EIT media. We compare our model with experimental data from Ref. [4] and find good agreement. We then show how this system can generate a regular train of single photons from uniform coherent-state input. Such photon trains have wide utility in applications such as boson sampling [28], quantum key distribution [29], and sub-shot-noise imaging of low-absorption samples [30]. At a more fundamental level, the emergence of a strongly correlated state of photons from a classical input is an interesting case study for emergent behavior in non-equilibrium quantum many-body systems.

In a simplistic picture of the high-intensity dynamics

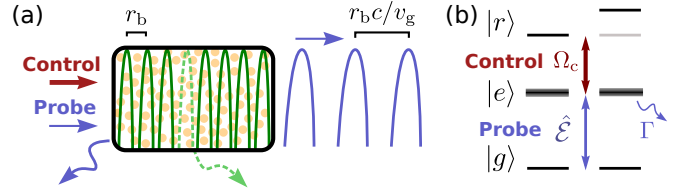


Figure 1. Dissipative Rydberg blockade in a one-dimensional atomic EIT medium. (a) Dynamics resulting from high-intensity CW probing according to naive expectation. The one-dimensional wave train of polaritons and outgoing photons is indicated. (b) Level diagram for the atoms leading to a dissipative blockade. Ground and Rydberg levels,  $|g\rangle$  and  $|r\rangle$ , are long-lived compared to the lossy excited level  $|e\rangle$  with decay rate  $2\Gamma$ . Outside the blockade radius of Rydberg polaritons, an incoming photon enjoys EIT transmission (left set of energy levels). For atoms within the blockade region of a polariton, the Rydberg level  $|r\rangle$  is shifted out of resonance with respect to the classical drive  $\Omega_c$  causing an incoming photon to scatter out of the excited state  $|e\rangle$ .

of such a medium [Fig. 1(a)], a bright continuous-wave (CW) probe field produces a train of Rydberg polaritons (green peaks). Via Rydberg-Rydberg (R-R) interactions, one polariton destroys lossless EIT-propagation conditions for other nearby polaritons. As a result, inside the medium, the polaritons are separated by their blockade radius  $r_b$  due to the scattering of “superfluous” photons at the entrance (purple wavy arrow) out of the forward-propagating mode. In turn, the polaritons exit the medium as a train of single photons spaced by the decompressed blockade radius  $r_b c/v_g$  ( $v_g$  is the polariton group velocity and  $c$  is the speed of light). However, polaritons may decay (green dashed arrow) due to the finite

width of the EIT window [4], whereby the observed anti-bunching feature will have an extent which significantly exceeds the blockade time  $\tau_b \equiv r_b/v_g$ . This is due to the spectral features of width  $\sim 1/\tau_b$  generated by the blockade exceeding the bandwidth of the EIT transmission window. Consequently, these features are washed out due to EIT filtering as the polaritons propagate through the medium. We include in our model this detrimental *single-polariton* EIT effect, that sets the limits of control for Rydberg-EIT media, but has been ignored in existing theories for the high-intensity regime.

Rydberg-EIT blockade experiments have been performed in both free space [1, 3–5, 31] and intra-cavity [32] settings. Focusing here on the former, a number of theoretical approaches to the dissipative blockade can be found in the literature: Theories based on semi-classical weak probing [33] and quantum super atoms [34–36], respectively, have both successfully predicted the experimental transmission data of Ref. [1]. Also accounting for the quantum nature of light, Ref. [13] analyzed the case of two strongly interacting photons. Here it was demonstrated that dissipative Rydberg-EIT media subject to copropagating input photons will produce an output field exhibiting the avoided volume associated with blockade, an effect that may serve as the basis of a single-photon filter in the limit of large optical depth per blockade radius  $d_b \gg 1$  [6].

Our model has two main advantages over previous work in this direction [6]: Firstly, by allowing for input pulses exceeding the blockade time  $\tau_b$ , we can analyze the CW limit of operation. Secondly, we incorporate the fact that single-polariton EIT decay releases the blockade, thereby allowing for the formation of a new polariton.

To set up the model, we start by considering the limit of perfect single-polariton EIT,  $d_b \gg 1$ , allowing us to discuss the R-R interactions independently. These arise in an ensemble of 3-level atoms in the ladder configuration [Fig. 1(b)], in which the van der Waals potential associated with a Rydberg excitation  $|r\rangle$  tunes neighboring atoms out of the EIT condition, thus activating the dissipation channel of the excited state  $|e\rangle$ . For simplicity, we replace the potential by a hard-sphere potential of radius  $r_b$  such that inside this region the photons immediately scatter, whereas outside they are unaffected.

Within this hard-sphere model, the action of the Rydberg medium on a pulsed input can be understood as sketched in Fig. 2: If a photon successfully enters the medium, it forms a polariton propagating without loss at speed  $v_g$ . If another photon enters at time  $\tau_1 < \tau_b$  after the polariton was created, it will scatter out of the forward-propagating mode. As a result, the environment effectively projects the wave function of the polariton to be localized within the arrival time interval  $[\tau_1 - \tau_b, \tau_1]$  [see Fig. 2(a)]. As long as the polariton is within the first blockade radius of the entrance, subse-

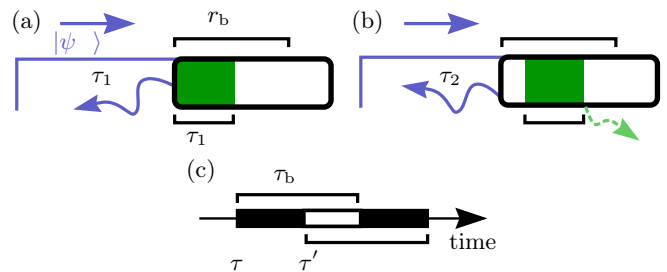


Figure 2. Formation of the polariton wave function by projection of an incoming pulse in state  $|\psi_{in}\rangle$  according to the hard-sphere model in the limit of perfect single-polariton EIT. (a) An incoming probe photon is scattered at time  $\tau_1$  thereby creating a polariton pulse (green rectangle) in the medium. (b) This pulse propagates further into the medium until at a time  $\tau_2$  a second probe photon scatters, but since (in this instance) the polariton could not have left the first  $r_b$  of the medium, no additional projection of the polariton wave function ensues (see [37] for an extended discussion). The short duration of the polariton leads to EIT losses (green dashed arrow). (c) Geometrical derivation of polariton coherence: The overlap of the blockade regions during arrival times  $\tau$  and  $\tau'$  is indicated by shading. The “forbidden” region, during which scattering events would ruin the superposition between  $\tau$  and  $\tau'$ , is shown in black (here assuming  $|\tau - \tau'| \leq \tau_b$ ).

quent scattering events will not further localize the polariton [see Fig. 2(b)]; hence, only the single-polariton physics plays a role during the propagation through this region. Once the polariton has propagated a distance  $r_b$  into the medium, it can no longer cause scattering of incoming photons and a new polariton may be formed at the entrance of the medium [38]. When a polariton reaches the rear of the medium, it will map back onto the outgoing optical field after undergoing spatial decompression by a factor of  $c/v_g$ .

*Dissipative theory at high intensity.*—We will now apply these ideas to analyze two scenarios involving dissipative Rydberg-EIT media in the one-dimensional limit, where the transverse spot size of the impinging light fields is small compared to  $r_b$ . As our first application, we consider the transmission behavior for a medium subject to CW probe and control fields as a function of the input rate  $\mathcal{R}_{in}$  of the probe.

Preliminarily, we derive the output rate in absence of single-polariton EIT decay, i.e., only considering the R-R interaction. The input rate  $\mathcal{R}_{in}$  splits into two fractions, the rate of photons that make it through the medium  $\mathcal{R}_{out}$  and a rate of R-R scattered photons,  $\mathcal{R}_{out}\tau_b\mathcal{R}_{in}$  [39]:

$$\mathcal{R}_{in} = \mathcal{R}_{out} + \mathcal{R}_{out}\tau_b\mathcal{R}_{in}; \quad (1)$$

$\tau_b\mathcal{R}_{in}$  is the average number of photons scattered by each Rydberg polariton, while  $\mathcal{R}_{out}$  is the rate of periods where the medium is blockaded. From Eq. (1), we

find the desired result [40]

$$\mathcal{R}_{\text{out}} = \frac{1}{\tau_b + 1/\mathcal{R}_{\text{in}}}. \quad (2)$$

As expected, the output rate  $\mathcal{R}_{\text{out}}$  is upper-bounded by both the input rate  $\mathcal{R}_{\text{in}}$  and the inverse blockade time  $1/\tau_b$ , with each bound achievable in the limit of weak blockade  $\tau_b \rightarrow 0$  and high input rate  $\mathcal{R}_{\text{in}} \rightarrow \infty$ , respectively.

We now turn to the more realistic case of imperfect single-polariton EIT, in which we must account for the finite transmission of polaritons that do not fit within the EIT window. If a polariton is EIT-scattered within the first blockade radius  $r_b$  of the medium, its blocking effect ceases, hence allowing for the creation of a new polariton at the input of the medium. Therefore the average blockade time per polariton  $\bar{\tau}_b$  is upper-bounded by that of a polariton that makes it through the first  $r_b$  of the medium,  $\bar{\tau}_b \leq \tau_b$ . Introducing the average single-polariton EIT transmission  $\bar{\eta}_{\text{EIT}}(L)$  through a medium of length  $L \geq r_b$  and the average Rydberg formation rate  $\mathcal{R}_{\text{Rf}}$ , we decompose the input rate in the spirit of Eq. (1),

$$\mathcal{R}_{\text{in}} = \bar{\eta}_{\text{EIT}}(L)\mathcal{R}_{\text{Rf}} + [1 - \bar{\eta}_{\text{EIT}}(L)]\mathcal{R}_{\text{Rf}} + \mathcal{R}_{\text{Rf}}\bar{\tau}_b\mathcal{R}_{\text{in}}, \quad (3)$$

where on the right-hand side the first term is the output rate,  $\mathcal{R}_{\text{out}} \equiv \bar{\eta}_{\text{EIT}}(L)\mathcal{R}_{\text{Rf}}$ , the second term is the rate of polariton EIT decay, and the third term is the rate of R-R scattering events. Introducing the output rate  $\mathcal{R}_{\text{out}}$  into Eq. (3) and solving for this quantity, we find

$$\mathcal{R}_{\text{out}} = \frac{\bar{\eta}_{\text{EIT}}(L)}{\bar{\tau}_b + 1/\mathcal{R}_{\text{in}}}, \quad (4)$$

generalizing Eq. (2). Equation (4) shows that EIT decay alters the transmission not only by the trivial damping prefactor  $\bar{\eta}_{\text{EIT}}$ , but also by decreasing the effective blockade time  $\bar{\tau}_b \leq \tau_b$ . Moreover, since both  $\bar{\eta}_{\text{EIT}}$  and  $\bar{\tau}_b$  are likely to decrease with increasing  $\mathcal{R}_{\text{in}}$ , the transmission curve (4) need not be a monotonic function of  $\mathcal{R}_{\text{in}}$ .

To evaluate Eq. (4), we estimate  $\bar{\eta}_{\text{EIT}}(L)$  and  $\bar{\tau}_b$  using the idea of projection-free propagation discussed in connection with Fig. 2(a,b). This allows a serialized treatment: We take the temporal extent  $\tau$  of a polariton to be defined by the first R-R event after its formation and average over the Poisson distribution for the arrival times of photons. The associated EIT transmission is then modeled by that of a square pulse of duration  $\tau$  subjected to Gaussian filtering, yielding the following expressions [37],

$$\bar{\eta}_{\text{EIT}}(l) = \exp([\tau_{\text{EIT}}(l)\mathcal{R}_{\text{in}}]^2) \operatorname{erfc}(\tau_{\text{EIT}}(l)\mathcal{R}_{\text{in}}), \quad (5)$$

$$\frac{\bar{\tau}_b}{\tau_b} = \int_0^{r_b} \frac{dl}{r_b} \bar{\eta}_{\text{EIT}}(l) = \frac{\bar{\eta}_{\text{EIT}}(r_b) + \sqrt{\frac{4}{\pi}}\tau_{\text{EIT}}(r_b)\mathcal{R}_{\text{in}} - 1}{[\tau_{\text{EIT}}(r_b)\mathcal{R}_{\text{in}}]^2}, \quad (6)$$

where the full blockade time is  $\tau_b = d_b/(2\gamma_{\text{EIT}})$ , the filtering time  $\tau_{\text{EIT}}(l) \equiv \sqrt{d_b l/r_b}/\gamma_{\text{EIT}}$  and  $\gamma_{\text{EIT}} \equiv \Omega_c^2/\Gamma$

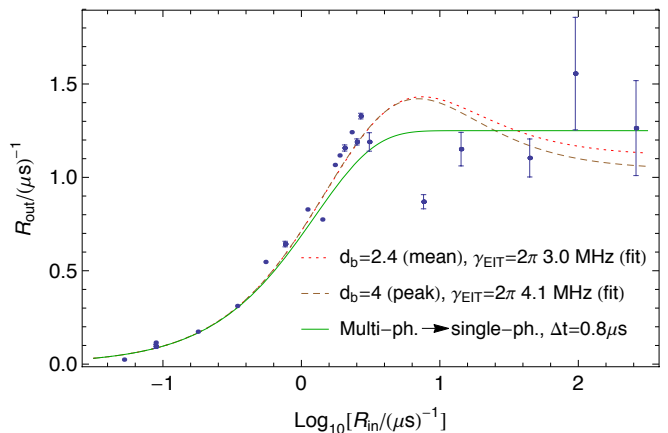


Figure 3. Transmission through a dissipative Rydberg-EIT medium. Output rate  $\mathcal{R}_{\text{out}}$  as function of input rate  $\mathcal{R}_{\text{in}}$ . The data from Ref. [4] is compared to plots of Eq. (4) for two fixed values of  $d_b$  corresponding to mean (red dotted) and peak (brown dashed) values of the Gaussian atomic density distribution in the experiment with axial spread  $\sigma_{\text{ax}}$  and effective length  $L = 4.2 \times \sigma_{\text{ax}}$ . The value for the single-atom EIT linewidth in the experiment was  $\gamma_{\text{EIT}} = 2\pi \times 7.5$  MHz. Also plotted (solid green curve) is the rate resulting from converting all multi-photon events within successive time intervals  $\Delta t = 0.8 \mu\text{s}$  into single-photon events  $\mathcal{R}_{\text{out}} = (\Delta t)^{-1}(1 - e^{-\mathcal{R}_{\text{in}}\Delta t})$ . The latter was presented alongside the data in Ref. [4].

is the single-atom EIT linewidth in terms of the control field Rabi frequency  $\Omega_c$  and the halfwidth  $\Gamma$  of the intermediate level [41]; taken together with these definitions, Eqs. (5,6) determine the output rate (4).

We plot Eq. (4) in Fig. 3 using the experimental parameters of Ref. [4] and compare to the data and the alternative theoretical curve presented therein (however,  $\gamma_{\text{EIT}}$  was obtained by fitting Eq. (4) to the data resulting in values within a factor of 2 from that cited in Ref. [4]). Within the error bars of the data, Eq. (4) is seen to match the data equally well as the theoretical curve proposed in Ref. [4]. Crucially, however, the physics implicit in the latter functional form is at odds with that of the Rydberg blockade: It puts no lower limit on the spacing between output photons, and the time-scale  $\Delta t$  that must be assumed to fit the data is an order of magnitude larger than  $\tau_b$  calculated from experimental parameters. Eq. (4) predicts the following two features of the transmission curve: Firstly, a finite asymptote for the limit of very high intensity,  $\mathcal{R}_{\text{in}} \rightarrow \infty$ ; while in this limit the average transmission probability goes to zero,  $\bar{\eta}_{\text{EIT}}(L) \rightarrow 0$ , the effective blockade time will likewise decrease,  $\bar{\tau}_b \rightarrow 0$ , thereby increasing the polariton formation rate in a manner such that  $\mathcal{R}_{\text{out}}$  in Eq. (4) remains finite. Secondly, Eq. (4) in general exhibits a local maximum as in Fig. 3.

*Generation of a single-photon train.*—We will now show that, in the limit  $d_b \gg 1$ , a CW probe gets con-

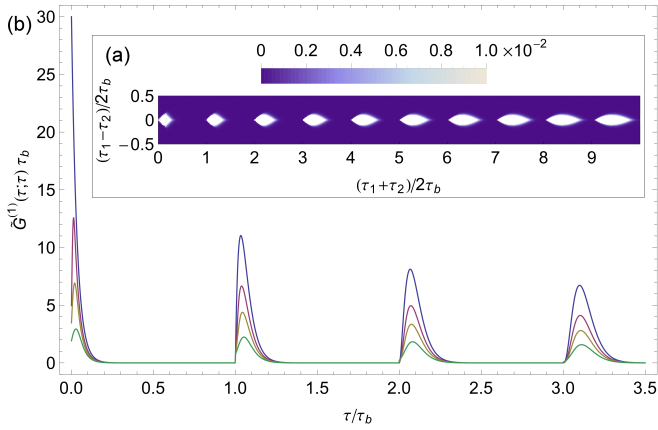


Figure 4. (a)  $G^{(1)}(\tau_1; \tau_2)$  [in units of  $1/\tau_b$ ] for coherent square-pulse input entering the medium at  $\tau = 0$  in the limit of perfect single-polariton EIT, Eq. (8) with  $\mathcal{R}_{\text{in}} = 30/\tau_b$  (values  $> 10^{-2}$  are plotted as white for illustrative purposes). (b) Diagonal elements of the EIT-filtered correlation function  $\hat{G}^{(1)}(\tau; \tau)$  for EIT width  $1/\tau_{\text{EIT}}$ , where  $\tau_{\text{EIT}}\mathcal{R}_{\text{in}} \in \{0, 1/4, 1/2, 1\}$  (in order of decreasing amplitude: purple, magenta, yellow, green).

verted into a regular pulse train of single photons [see Fig. 1(a)]. The blockade sets a lower limit  $\tau_b$  to the temporal separation of output photons leading to anti-bunching. To achieve regularity, we must also impose an upper bound on the (average) separation. This can be ensured by a sufficiently large input rate, but only insofar as single-polariton EIT decay remains rare. Such a decay event will terminate the regularity of the pulse train (creating a “domain wall”), effectively resetting the process. These considerations imply that an optimum input rate exists as a trade-off between the input photons not being too far apart (on average) while keeping single-polariton EIT decay at a perturbative level. In this regime, we may take  $\bar{\tau}_b \approx \tau_b$  and estimate  $\bar{\eta}_{\text{EIT}}$  by filtering the correlation functions  $G^{(1)}(\tau; \tau') = \langle \hat{\mathcal{E}}^\dagger(\tau)\hat{\mathcal{E}}(\tau') \rangle$  produced by the idealized R-R interaction [see Fig. 2(a,b)] (as was checked by numerical simulations [37]).

We first derive the diagonal element  $G^{(1)}(\tau; \tau)$  by observing that its value at a time  $\tau$  after the onset of the pulse can have contributions from at most  $\lceil \tau/\tau_b \rceil$  polaritons per the hard-sphere ansatz. The contribution from each polariton follows from straightforward integration of the Poisson distribution; we then find ( $\tau \geq 0$ ) [37]

$$G^{(1)}(\tau; \tau) = \sum_{j=0}^{\lceil \tau/\tau_b \rceil} \mathcal{R}_{\text{in}} e^{-\mathcal{R}_{\text{in}}(\tau - j\tau_b)} \frac{[\mathcal{R}_{\text{in}}(\tau - j\tau_b)]^j}{j!} \quad (7)$$

(the argument can be extended to obtain higher-order correlation functions [37]). This function is plotted in Fig. 4(b) (top blue curve) in the high-intensity regime in which the statistical uncertainty in the creation time of polaritons is small (relative to  $\tau_b$ ); i.e., when only the term  $j = \lceil \tau/\tau_b \rceil$  in Eq. (7) contributes significantly.

The first-order correlation function  $G^{(1)}(\tau; \tau')$  quantifies the quantum coherence between having a Rydberg excitation at different times. This can be related to the diagonal elements  $G^{(1)}(\tau''; \tau'')$  by noting that  $G^{(1)}(\tau; \tau')$  is the probability density for the creation of a polariton at time  $\tau_{<} \equiv \min\{\tau, \tau'\}$  multiplied by the probability that no scattering events occur that allow the environment to distinguish whether the polariton was created at  $\tau$  or  $\tau'$ . From Fig. 2(c) we see that this requires that no photons impinge on the medium for intervals of combined duration  $2|\tau - \tau'|$  [42], which is all the information needed for Poisson-distributed input (here focusing on  $|\tau - \tau'| \leq \tau_b$  relevant for the limit of interest,  $d_b \gg 1$ , in which  $\tau_{\text{EIT}} \ll \tau_b$ ). Hence ( $|\tau - \tau'| \leq \tau_b$ )

$$G^{(1)}(\tau; \tau') = G^{(1)}(\tau_{<}; \tau_{<}) e^{-2\mathcal{R}_{\text{in}}|\tau - \tau'|}, \quad (8)$$

where the diagonal elements of  $G^{(1)}$  are given by Eq. (7). Equation (8) is plotted in Fig. 4(a). By convolving Eq. (8) with a Gaussian filter function corresponding to a medium of length  $L = \tau_b$ , we estimate the effect of EIT decay, obtaining the intensity profile  $\hat{G}^{(1)}(\tau; \tau)$  plotted in Fig. 4(b).

Equation (7) captures how the accumulated randomness in the photon arrival times determines the spread in the formation times of polaritons. To obtain a parameter condition ensuring regularity of the pulse train for the first  $N_{\text{loc}}$  peaks of  $G^{(1)}(\tau; \tau')$ , we demand that the width  $(\delta t)_N$  of the widest peak in the train obeys  $(\delta t)_N \leq \beta\tau_b$  for some fraction  $\beta$  of  $\tau_b$ , yielding the requirement ( $N_{\text{loc}} \gg 1$ )  $\mathcal{R}_{\text{in}} \gtrsim \sqrt{N_{\text{loc}}}/(\beta\tau_b)$  [37]. On the other hand, if we can tolerate an EIT loss fraction of at most  $\epsilon = 1 - \bar{\eta}_{\text{EIT}}$ , filtering Eq. (8) yields an upper bound (in the limit  $\tau_{\text{EIT}} \ll 1/\mathcal{R}_{\text{in}}, \tau_b$ ),  $\mathcal{R}_{\text{in}} \lesssim 1/(N_{\text{EIT}}\tau_{\text{EIT}})$ , where  $N_{\text{EIT}} \sim 1/\epsilon$  is the average pulse train length allowed by the EIT filter. Balancing these two considerations by setting  $N = N_{\text{loc}} = N_{\text{EIT}}$  and seeking its maximal value  $N_{\text{max}}$  that permits the simultaneous fulfillment of the above requirements, we find

$$N_{\text{max}} \sim \sqrt[3]{\frac{\pi\beta^2}{128 \ln 2} d_b}, \quad (9)$$

having used  $\tau_b = d_b/(2\gamma_{\text{EIT}})$  and  $\tau_{\text{EIT}} = \sqrt{d_b}/\gamma_{\text{EIT}}$ . For this expression to reach  $N_{\text{max}} \gtrsim 1$  requires  $d_b \gtrsim 100$  for  $\beta \approx 1/2$  and hence we find the generation of single-photon pulse trains to demand very large  $d_b$ . The scaling behavior (9) resulting from the limiting effects identified here may be improved by directing the scattered light into well defined channels using cooperative light emission [43].

In conclusion, we have proposed a new model for analyzing the many-body physics of the dissipative Rydberg blockade in extended one-dimensional EIT media. The work presented here may serve as a guide for the rigorous derivation of effective many-body theories [44]. In this regard, we remark that ongoing work on numerically simulating Rydberg-EIT media using matrix product states



yields results which are in qualitative agreement with the present work [45, 46].

One can envision several extensions of our approach: Storage and retrieval operations in Rydberg media can be modeled by translating time-varying control fields into a time-dependent blockade time  $\tau_b$  of hard-sphere Rydberg polaritons. In three-dimensional Rydberg media, multi-body Rydberg scattering events can take place when the blockade regions of transversely spaced polaritons overlap. It would also be intriguing to consider whether our protocol for the generation of photon trains can be modified, perhaps by employing cooperative resonances in regular atomic arrays [47], to turn the photon trains into time crystals [48, 49] that keep their periodicity for times that are exponentially long in the input intensity.

E.Z. is grateful to J. Taylor and the Joint Quantum Institute for hosting him during the time when this project was conceived. We thank the Vuletić-Lukin group for providing their experimental data. We thank Q.-Y. Liang, J. Thompson, V. Vuletić, M. Lukin, J. Taylor, O. Firstenberg, T. Pohl, C. Murray, S. Hofferberth, D. Chang, N. Yao, and C. Nayak for discussions. E.Z. acknowledges funding from the European Research Council under the European Union Seventh Framework Programme (FP/2007-2013) / European Research Council Grant Agreement No. 306576 and the Carlsberg Foundation. M. J. G., M. F. M., and A. V. G. thank the following funding sources: Army Research Laboratory Center for Distributed Quantum Information, National Science Foundation Quantum Information Science program, National Science Foundation Physics Frontier Center at the Joint Quantum Institute, Air Force Office of Scientific Research, Army Research Office, and Army Research Office Multidisciplinary University Research Initiative. M. F. M. acknowledges start-up funding from Michigan State University. W. H. P. Nielsen provided graphical assistance.

---

\* zeuthen@nbi.ku.dk

- [1] J. D. Pritchard, D. Maxwell, A. Gauguier, K. J. Weatherill, M. P. A. Jones, and C. S. Adams, “Cooperative atom-light interaction in a blockaded rydberg ensemble,” *Phys. Rev. Lett.* **105**, 193603 (2010).
- [2] David Petrosyan, Johannes Otterbach, and Michael Fleischhauer, “Electromagnetically induced transparency with rydberg atoms,” *Phys. Rev. Lett.* **107**, 213601 (2011).
- [3] Y. O. Dudin and A. Kuzmich, “Strongly interacting rydberg excitations of a cold atomic gas,” *Science* **336**, 887–889 (2012).
- [4] Thibault Peyronel, Ofer Firstenberg, Qi-Yu Liang, Sebastian Hofferberth, Alexey V. Gorshkov, Thomas Pohl, Mikhail D. Lukin, and Vladan Vuletic, “Quantum nonlinear optics with single photons enabled by strongly interacting atoms,” *Nature* **488**, 57–60 (2012).
- [5] D. Maxwell, D. J. Szwer, D. Paredes-Barato, H. Busche, J. D. Pritchard, A. Gauguier, K. J. Weatherill, M. P. A. Jones, and C. S. Adams, “Storage and control of optical photons using rydberg polaritons,” *Phys. Rev. Lett.* **110**, 103001 (2013).
- [6] Alexey V. Gorshkov, Rejish Nath, and Thomas Pohl, “Dissipative many-body quantum optics in rydberg media,” *Phys. Rev. Lett.* **110**, 153601 (2013).
- [7] Ofer Firstenberg, Thibault Peyronel, Qi-Yu Liang, Alexey V. Gorshkov, Mikhail D. Lukin, and Vladan Vuletic, “Attractive photons in a quantum nonlinear medium,” *Nature (London)* **502**, 71 (2013).
- [8] P. Bienias, S. Choi, O. Firstenberg, M. F. Maghrebi, M. Gullans, M. D. Lukin, A. V. Gorshkov, and H. P. Büchler, “Scattering resonances and bound states for strongly interacting rydberg polaritons,” *Phys. Rev. A* **90**, 053804 (2014).
- [9] M. F. Maghrebi, M. J. Gullans, P. Bienias, S. Choi, I. Martin, O. Firstenberg, M. D. Lukin, H. P. Büchler, and A. V. Gorshkov, “Coulomb bound states of strongly interacting photons,” *Phys. Rev. Lett.* **115**, 123601 (2015).
- [10] M. D. Lukin, M. Fleischhauer, R. Cote, L. M. Duan, D. Jaksch, J. I. Cirac, and P. Zoller, “Dipole blockade and quantum information processing in mesoscopic atomic ensembles,” *Phys. Rev. Lett.* **87**, 037901 (2001).
- [11] Daniel Comparat and Pierre Pillet, “Dipole blockade in a cold rydberg atomic sample [invited],” *J. Opt. Soc. Am. B* **27**, A208–A232 (2010).
- [12] Michael Fleischhauer, Atac Imamoglu, and Jonathan P. Marangos, “Electromagnetically induced transparency: Optics in coherent media,” *Rev. Mod. Phys.* **77**, 633–673 (2005).
- [13] Alexey V. Gorshkov, Johannes Otterbach, Michael Fleischhauer, Thomas Pohl, and Mikhail D. Lukin, “Photon-photon interactions via rydberg blockade,” *Phys. Rev. Lett.* **107**, 133602 (2011).
- [14] Ephraim Shahmoon, Gershon Kurizki, Michael Fleischhauer, and David Petrosyan, “Strongly interacting photons in hollow-core waveguides,” *Phys. Rev. A* **83**, 033806 (2011).
- [15] D. Paredes-Barato and C. S. Adams, “All-optical quantum information processing using rydberg gates,” *Phys. Rev. Lett.* **112**, 040501 (2014).
- [16] Daniel Tiarks, Steffen Schmidt, Gerhard Rempe, and Stephan Dürr, “Optical  $\pi$  phase shift created with a single-photon pulse,” *Sci. Adv.* **2**, e1600036–e1600036 (2016).
- [17] Daniel Tiarks, Simon Baur, Katharina Schneider, Stephan Dürr, and Gerhard Rempe, “Single-Photon Transistor Using a Förster Resonance,” *Phys. Rev. Lett.* **113**, 053602 (2014).
- [18] H. Gorniaczyk, C. Tresp, J. Schmidt, H. Fedder, and S. Hofferberth, “Single-photon transistor mediated by interstate Rydberg interactions,” *Phys. Rev. Lett.* **113**, 053601 (2014).
- [19] D. Maxwell, D. J. Szwer, D. Paredes-Barato, H. Busche, J. D. Pritchard, A. Gauguier, M. P. A. Jones, and C. S. Adams, “Microwave control of the interaction between two optical photons,” *Phys. Rev. A* **89**, 043827 (2014).
- [20] Anne E. B. Nielsen and Klaus Mølmer, “Deterministic multimode photonic device for quantum-information processing,” *Phys. Rev. A* **81**, 043822 (2010).
- [21] T. Pohl, E. Demler, and M. D. Lukin, “Dynamical crys-

- tallization in the dipole blockade of ultracold atoms,” *Phys. Rev. Lett.* **104**, 043002 (2010).
- [22] F. Bariani, Y. O. Dudin, T. A. B. Kennedy, and A. Kuzmich, “Dephasing of multiparticle rydberg excitations for fast entanglement generation,” *Phys. Rev. Lett.* **108**, 030501 (2012).
- [23] J. D. Pritchard, C. S. Adams, and K. Mølmer, “Correlated photon emission from multiatom rydberg dark states,” *Phys. Rev. Lett.* **108**, 043601 (2012).
- [24] Jovica Stanojevic, Valentina Parigi, Erwan Bimbard, Alexei Ourjoumtsev, Pierre Pillet, and Philippe Grangier, “Generating non-gaussian states using collisions between rydberg polaritons,” *Phys. Rev. A* **86**, 021403 (2012).
- [25] A Grankin, E Brion, E Bimbard, R Boddeda, I Usmani, A Ourjoumtsev, and P Grangier, “Quantum statistics of light transmitted through an intracavity rydberg medium,” *New Journal of Physics* **16**, 043020 (2014).
- [26] Mohammad F. Maghrebi, Norman Y. Yao, Mohammad Hafezi, Thomas Pohl, Ofer Firstenberg, and Alexey V. Gorshkov, “Fractional quantum hall states of rydberg polaritons,” *Phys. Rev. A* **91**, 033838 (2015).
- [27] S. Hofferberth, Private communication.
- [28] Keith R. Motes, Alexei Gilchrist, Jonathan P. Dowling, and Peter P. Rohde, “Scalable boson sampling with time-bin encoding using a loop-based architecture,” *Phys. Rev. Lett.* **113**, 120501 (2014).
- [29] P. Zoller, T. Beth, D. Binosi, R. Blatt, H. Briegel, D. Bruss, T. Calarco, J. I. Cirac, D. Deutsch, J. Eisert, A. Ekert, C. Fabre, N. Gisin, P. Grangiere, M. Grassl, S. Haroche, A. Imamoglu, A. Karlson, J. Kempe, L. Kouwenhoven, S. Kroll, G. Leuchs, M. Lewenstein, D. Loss, N. Lutkenhaus, S. Massar, J. E. Mooij, M. B. Plenio, E. Polzik, S. Popescu, G. Rempe, A. Sergienko, D. Suter, J. Twamley, G. Wendin, R. Werner, A. Winter, J. Wrachtrup, and A. Zeilinger, “Quantum information processing and communication - strategic report on current status, visions and goals for research in europe,” *Eur. Phys. J. D* **36**, 203 (2005).
- [30] G. Brida, M. Genovese, and I. Ruo Berchera, “Experimental realization of sub-shot-noise quantum imaging,” *Nat Photon* **4**, 227 (2010).
- [31] C. S. Hofmann, G. Günter, H. Schempp, M. Robert-de-Saint-Vincent, M. Gärttner, J. Evers, S. Whitlock, and M. Weidemüller, “Sub-poissonian statistics of rydberg-interacting dark-state polaritons,” *Phys. Rev. Lett.* **110**, 203601 (2013).
- [32] R Boddeda, I Usmani, E Bimbard, A Grankin, A Ourjoumtsev, E Brion, and P Grangier, “Rydberg-induced optical nonlinearities from a cold atomic ensemble trapped inside a cavity,” *Journal of Physics B: Atomic, Molecular and Optical Physics* **49**, 084005 (2016).
- [33] S. Sevinçli, N. Henkel, C. Ates, and T. Pohl, “Nonlocal nonlinear optics in cold rydberg gases,” *Phys. Rev. Lett.* **107**, 153001 (2011).
- [34] David Petrosyan, Johannes Otterbach, and Michael Fleischhauer, “Electromagnetically induced transparency with rydberg atoms,” *Phys. Rev. Lett.* **107**, 213601 (2011).
- [35] Yi-Mou Liu, Dong Yan, Xue-Dong Tian, Cui-Li Cui, and Jin-Hui Wu, “Electromagnetically induced transparency with cold rydberg atoms: Superatom model beyond the weak-probe approximation,” *Phys. Rev. A* **89**, 033839 (2014).
- [36] Martin Gärttner, Shannon Whitlock, David W. Schönleber, and Jörg Evers, “Semianalytical model for nonlinear absorption in strongly interacting rydberg gases,” *Phys. Rev. A* **89**, 063407 (2014).
- [37] See the Supplemental Material for detailed derivations of formulas and additional discussion.
- [38] Generally, this will lead to entanglement between polaritons and, hence, between the outgoing photons as discussed in the Supplemental Material.
- [39] We neglect finite-pulse corrections that arise from a finite averaging time.
- [40] Jörg W. Müller, “Some formulae for a dead-time-distorted poisson process: To andré allisy on the completion of his first half century,” *Nuclear Instruments and Methods* **117**, 401 – 404 (1974).
- [41]  $\tau_{\text{EIT}}$  is the inverse Gaussian width of the EIT amplitude filtering  $\propto \exp(-\omega^2 \tau_{\text{EIT}}^2 / 2)$  and the convention for  $\Omega_c$  is set by  $\partial_t \hat{P} = i\Omega_c \hat{S}$ , where  $\hat{P}$  and  $\hat{S}$  are the polarizations between  $|g\rangle-|e\rangle$  and  $|g\rangle-|r\rangle$  transitions, respectively.
- [42] Assuming  $\tau, \tau' \leq \tau_p - \tau_b$ , where  $\tau_p$  is the pulse duration.
- [43] Callum R. Murray and Thomas Pohl, “Coherent photon manipulation in interacting atomic ensembles,” *Phys. Rev. X* **7**, 031007 (2017).
- [44] M. J. Gullans, J. D. Thompson, Y. Wang, Q.-Y. Liang, V. Vuletić, M. D. Lukin, and A. V. Gorshkov, “Effective field theory for rydberg polaritons,” *Phys. Rev. Lett.* **117**, 113601 (2016).
- [45] Marco T. Manzoni, Darrick E. Chang, and James S. Douglas, “Simulating quantum light propagation through atomic ensembles using matrix product states,” *Nature Communications* **8**, 1743 (2017).
- [46] P. Bienias et al., in preparation.
- [47] Ephraim Shahmoon, Dominik S. Wild, Mikhail D. Lukin, and Susanne F. Yelin, “Cooperative resonances in light scattering from two-dimensional atomic arrays,” *Phys. Rev. Lett.* **118**, 113601 (2017).
- [48] Frank Wilczek, “Quantum time crystals,” *Phys. Rev. Lett.* **109**, 160401 (2012).
- [49] Alfred Shapere and Frank Wilczek, “Classical time crystals,” *Phys. Rev. Lett.* **109**, 160402 (2012).

# Supplemental Material for “Correlated photon dynamics in dissipative Rydberg media”

Emil Zeuthen,<sup>1,2,\*</sup> Michael J. Gullans,<sup>3</sup> Mohammad F. Maghrebi,<sup>3,4</sup> and Alexey V. Gorshkov<sup>3</sup>

<sup>1</sup>*Niels Bohr Institute, University of Copenhagen, DK-2100 Copenhagen, Denmark*

<sup>2</sup>*Institute for Theoretical Physics and Institute for Gravitational Physics (Albert Einstein Institute),  
Leibniz Universität Hannover, Callinstraße 38, 30167 Hannover, Germany*

<sup>3</sup>*Joint Quantum Institute and Joint Center for Quantum Information and Computer Science,  
National Institute of Standards and Technology and University of Maryland, College Park, Maryland 20742, USA*

<sup>4</sup>*Department of Physics and Astronomy, Michigan State University, East Lansing, Michigan 48824, USA*

## I. SUCCESSIVE PROJECTIONS OF THE POLARITON WAVE FUNCTION

In this Appendix, we comment further on the process by which the polariton wave train is generated in the medium. In particular, in Fig. 2(b) of the main text, we assumed that the second scattering event occurs when the polariton has not passed the first blockade radius of the medium. In this Appendix, we comment on what happens if a scattering event occurs when the polariton straddles the rear of the first blockade radius of the medium.

As discussed in the main text, the temporal extent of the polariton wave function is defined near the beginning of the medium [Fig. S1(a,b)]. Within the validity of the hard-sphere model, scattered photons are ignorant as to the precise distance to the scatterer, since the scattering event constitutes a projective, binary distance measurement. As a consequence, when a polariton (whose temporal extent was defined near the entrance) straddles the rear of the first blockade radius of the medium [Fig. S1(c)], then a scattering event cannot distinguish whether the scattering was caused by this distant polariton, or whether the distant polariton had already left and the scattering was instead caused by a newly formed polariton near the entrance [see Fig. S1(d)]. The resulting projection caused by the scattering hence acts simultaneously on the two polaritons leading to spatial entanglement [Fig. S1(d')].

As discussed in Appendix II, our model ignores such additional projections that can occur as the polariton leaves the first blockade radius of the medium. Since the rate of incoming photons determines both projection processes (the one occurring at the entrance into medium and the one occurring at the exit from the first blockade radius), we expect that ignoring the latter will not qualitatively affect our results.

## II. DETERMINATION OF TRANSMISSION FUNCTION

In this Appendix, we present the details behind the derivation of the expressions for the average EIT transmission  $\bar{\eta}_{\text{EIT}}(l)$  for a medium of length  $l$  and the average effective blockade time  $\bar{\tau}_b$  given in Eqs. (5) and (6) of the main text.

To estimate these quantities, we rely on the intuition presented in Fig. 2(a,b) of the main text: That the temporal extent of the polariton wave function is determined near the beginning of the medium by its first R-R scattering event, whereas subsequent propagation within the first blockade radius is unaffected by any additional R-R scattering events. This suggests a serialized treatment of the R-R scattering and single-polariton EIT-filtering. Applying this approach, we take the temporal extent  $\tau$  of a polariton to be defined by the first R-R event after its formation and assume its EIT transmission probability  $\eta_{\text{EIT}}(\tau, l)$  to be a function only of  $\tau$  and the propagation length  $l$  in the medium. In doing so, we ignore the additional projections that can occur as the polariton leaves the first blockade radius of the medium, as discussed in Appendix I.

Averaging the EIT transmission probability  $\eta_{\text{EIT}}(\tau, l)$  over the CW/Poisson distribution for the timing of the first R-R scattering event  $\tau$  amounts to

$$\bar{\eta}_{\text{EIT}}(l) = \langle \eta_{\text{EIT}}(\tau, l) \rangle_{\tau} = \int_0^{\infty} d\tau \mathcal{R}_{\text{in}}(\mathcal{R}_{\text{in}}\tau) e^{-\mathcal{R}_{\text{in}}\tau} \eta_{\text{EIT}}(\tau, l). \quad (\text{S1})$$

From this average transmission probability, we estimate the average effective blockade time as

$$\bar{\tau}_b = \tau_b \int_0^{\tau_b} \frac{dl}{\tau_b} \bar{\eta}_{\text{EIT}}(l). \quad (\text{S2})$$

---

\* zeuthen@nbi.ku.dk

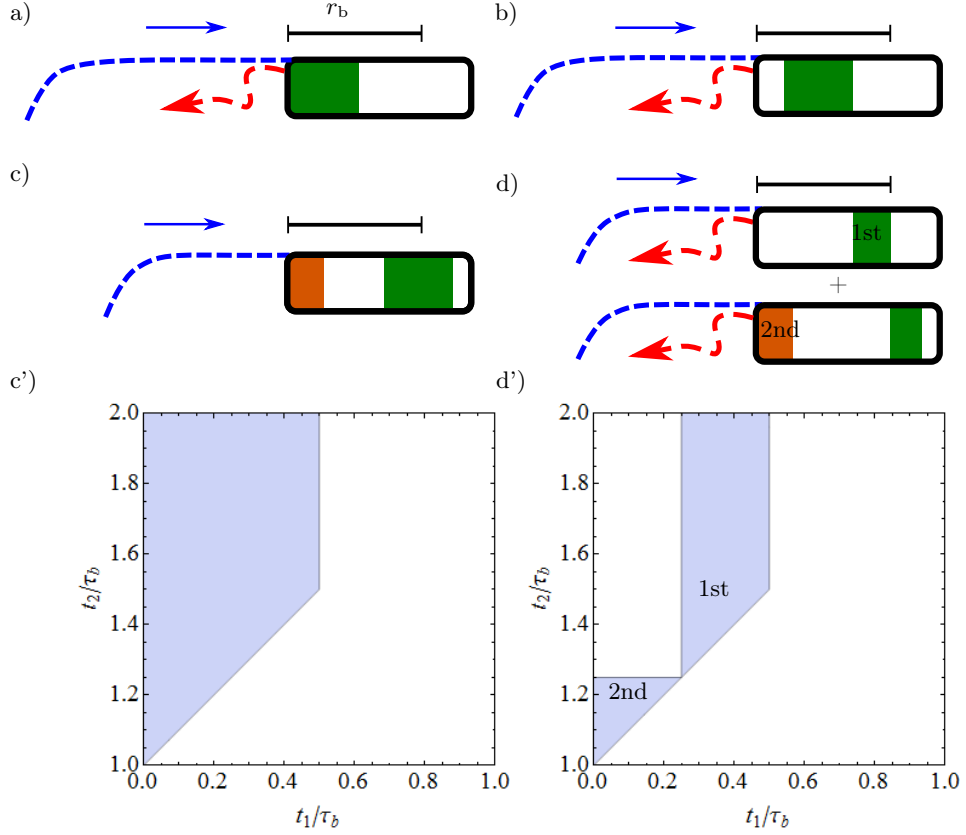


Figure S1. Formation of the polariton wave function by sequential projections of an incoming square pulse according to the hard-sphere model in the limit of perfect single-polariton EIT. (a) An incoming probe photon is scattered (red dashed arrow) near the beginning of the medium thereby projecting a polariton (green rectangle) in the medium. (b) The polariton propagates further into the medium, and, at a subsequent time, a second probe photon scatters, but since (in this instance) the polariton could not have left the first  $r_b$  of the medium, no additional projection of the polariton wave function ensues. (c) The polariton is now about to leave the first blockade radius of the medium, prompting us to consider possible formation times  $t_2$  of the second polariton as described by the two-photon wave function in (c'), assuming the pulse to arrive at  $t = 0$ . The shaded region denotes the support of the wavefunction. (d) The first and second polaritons straddle the rear and front boundaries of the first blockade radius as a scattering event occurs; this causes a projection (c')  $\rightarrow$  (d') on the two-body wave function producing a superposition state of the first and second polariton [as indicated in (d')] being the scatterer.

Approximating  $\eta_{\text{EIT}}(\tau, l)$  by the EIT transmission of a square pulse subjected to Gaussian filtering,

$$\eta_{\text{EIT}}(\tau, l) = \int_0^\tau dt_1 \int_0^\tau dt_2 \frac{1}{\tau \sqrt{4\pi} \tau_{\text{EIT}}(l)} \exp\left[-\frac{(t_1 - t_2)^2}{4\tau_{\text{EIT}}^2(l)}\right] = \text{Erf}\left[\frac{\tau}{2\tau_{\text{EIT}}(l)}\right] - \frac{2\tau_{\text{EIT}}(l)}{\sqrt{\pi}\tau} \left(1 - \exp\left[\frac{\tau^2}{4\tau_{\text{EIT}}^2(l)}\right]\right), \quad (\text{S3})$$

the integrals in Eqs. (S1,S2) can be evaluated, yielding the expressions given in Eqs. (5) and (6) of the main text.

### III. HARD-SPHERE CORRELATION FUNCTIONS

In this Appendix, we present the details behind the derivation of the first-order correlation function  $G^{(1)}(\tau; \tau')$  presented in Eq. (7) of the main text, plot  $G^{(1)}(\tau; \tau)$  for different parameters, and generalize the derivation to higher-order correlation functions. The derivations are carried out within the idealized hard-sphere dynamics for which single-polariton EIT effects are absent.

#### A. First-order correlation function

In this Section, we present the details behind the derivation of  $G^{(1)}(\tau; \tau)$ , Eq. (7) from the main text, and plot this function for different combinations of input rate and blockade time.



The same-time first-order correlation function  $G^{(1)}(\tau; \tau)$  is given by the ensemble-averaged intensity profile  $(\hat{I}(\tau))_{\hat{\rho}} = \langle \hat{\mathcal{E}}^\dagger(\tau) \hat{\mathcal{E}}(\tau) \rangle_{\hat{\rho}} = G^{(1)}(\tau; \tau)$ , where the subscript signifies expectation value with respect to the density matrix  $\hat{\rho}$  resulting from the hard-sphere interaction (ignoring EIT filtering). For square-pulse Poisson input (of rate  $\mathcal{R}_{\text{in}}$ ), this function can be derived inductively by propagating the initial condition that the medium is empty when the input pulse arrives at the medium at time  $\tau_s$  (and using the fact that different segments of the input pulse are uncorrelated). Let us first consider the probability density  $P_1(t_1 - \tau_s)$  of the first Rydberg excitation occurring at a time  $t_1 \geq \tau_s$ ; this is simply the product of the probability that no photons arrived during the interval  $[\tau_s; t_1]$ , i.e.  $\exp[-\mathcal{R}_{\text{in}}(t_1 - \tau_s)]$  for the Poisson distribution, and the arrival rate of photons  $\mathcal{R}_{\text{in}}$ , so that we have

$$P_1(\tau) = \theta(\tau) \mathcal{R}_{\text{in}} \exp[-r\tau], \quad (\text{S4})$$

where  $\theta(\tau)$  is the Heaviside step function with the convention  $\theta(0) = 1$ . Next, let us construct the probability density  $P_2(t_2 - \tau_s)$  that the second Rydberg excitation occurs at time  $t_2$ . Note that, per the hard-sphere ansatz, this probability density can be non-zero only for  $t_2 \geq \tau_s + \tau_b$ . The *conditional* probability density of the second Rydberg excitation occurring at  $t_2$  conditioned on the first Rydberg excitation arriving at  $t_1$  is just  $P_1(t_2 - t_1 - \tau_b)$ , where  $P_1$  is given in Eq. (S4); i.e. the first Rydberg excitation (at  $t_1$ ) imposes an initial condition of an empty medium at  $t_1 + \tau_b$  equivalent to the one at  $\tau_s$ . The unconditional probability density  $P_2(t_2 - \tau_s)$  for the arrival of the second Rydberg at  $t_2$  is then found by integrating the conditional density  $P_1(t_2 - t_1 - \tau_b)$  over  $t_1 \in [\tau_s, t_2 - \tau_b]$  weighted by the probability density  $P_1(t_1 - \tau_s)$  we found above for  $t_1$ ,

$$\begin{aligned} P_2(t_2 - \tau_s) &= \theta(t_2 - \tau_s - \tau_b) \int_{\tau_s}^{t_2 - \tau_b} dt_1 P_1(t_1 - \tau_s) \times P_1(t_2 - t_1 - \tau_b) \\ &= \theta(t_2 - \tau_s - \tau_b) \mathcal{R}_{\text{in}} \exp[-\mathcal{R}_{\text{in}}(t_2 - \tau_s - \tau_b)] \times [\mathcal{R}_{\text{in}}(t_2 - \tau_s - \tau_b)]. \end{aligned} \quad (\text{S5})$$

By iterating this argument, we find the probability density for the arrival of the  $R$ 'th Rydberg excitation at time  $t_R$  to be given by (defining  $t_0 \equiv \tau_s - \tau_b$  for convenience)

$$P_R(t_R - \tau_s) = \theta(t_R - \tau_s - (R-1)\tau_b) \mathcal{R}_{\text{in}} e^{-\mathcal{R}_{\text{in}}(t_R - \tau_s - (R-1)\tau_b)} \frac{[\mathcal{R}_{\text{in}}(t_R - \tau_s - (R-1)\tau_b)]^{R-1}}{(R-1)!}. \quad (\text{S6})$$

$P_R(t_R - \tau_s)$  in Eq. (S6) is the probability density of the creation of a polariton at time  $t_R$  conditioned on  $R-1$  polaritons having been created in the preceding time interval  $[\tau_s, t_R - \tau_b]$ . This allows us to construct  $G^{(1)}(\tau; \tau)$  simply by observing that its value at a time  $\tau = t - \tau_s$  after the onset of the pulse only can have contributions from the first  $\lceil (t - \tau_s)/\tau_b \rceil$  polaritons created since  $\tau_s$  per the hard-sphere ansatz; summing these contributions, Eq. (S6), we find ( $t \geq \tau_s$ )

$$G^{(1)}(t - \tau_s; t - \tau_s) = \sum_{j=1}^{\lceil (t - \tau_s)/\tau_b \rceil} P_j(t - \tau_s) = \sum_{j'=0}^{\lfloor (t - \tau_s)/\tau_b \rfloor} \mathcal{R}_{\text{in}} e^{-\mathcal{R}_{\text{in}}(t - \tau_s - j'\tau_b)} \frac{[\mathcal{R}_{\text{in}}(t - \tau_s - j'\tau_b)]^{j'}}{j'!}, \quad (\text{S7})$$

also given in Eq. (7) of the main text (setting  $\tau_s = 0$  for simplicity). We plot Eq. (S7) in Fig. S2 for different combinations of the input rate  $\mathcal{R}_{\text{in}}$  and the blockade time in units of pulse duration  $\tau_b/\tau_p$ . The width of the peaks are seen to increase with peak number while their heights decrease. This is a symptom of the decay of the initial condition of a vacant medium at  $\tau_s$  when the pulse arrives, corresponding to the decay of photon-photon correlations in the output signal.

The off-diagonal elements  $G^{(1)}(t - \tau_s; t' - \tau_s)$  can be expressed conveniently in terms of the diagonal elements (S7)

$$G^{(1)}(t - \tau_s; t' - \tau_s) = G^{(1)}(t_{<} - \tau_s; t_{<} - \tau_s) e^{-2\mathcal{R}_{\text{in}} \min\{|t - t'|, \tau_b\}} \times \begin{cases} 1, & \text{if } |t - t'| \leq \tau_b \\ \mathcal{R}_{\text{in}}^{-1} G^{(1)}(|t - t'| - \tau_b; |t - t'| - \tau_b), & \text{if } |t - t'| > \tau_b \end{cases}, \quad (\text{S8})$$

where  $t_{<} \equiv \min\{t, t'\}$ . Eq. (S8) is derived in the main text for the special case  $|t - t'| \leq \tau_b$ , see Eq. (8). In the case  $|t - t'| > \tau_b$  we must account for the fact that not all event histories for the intermediate time interval  $[\min\{t, t'\} + \tau_b; \max\{t, t'\}]$  are compatible with the medium being vacant at  $\max\{t, t'\}$ ; hence we multiply by the probability that this is the case conditioned on the medium being vacant at  $\min\{t, t'\} + \tau_b$ , i.e.,  $\mathcal{R}_{\text{in}}^{-1} G^{(1)}(|t - t'| - \tau_b; |t - t'| - \tau_b)$ .

## B. Higher-order correlation functions

In this Section, we extend the arguments of the previous section to derive higher-order correlation functions, a possibility mentioned in conjunction with Eq. (7) of the main text.

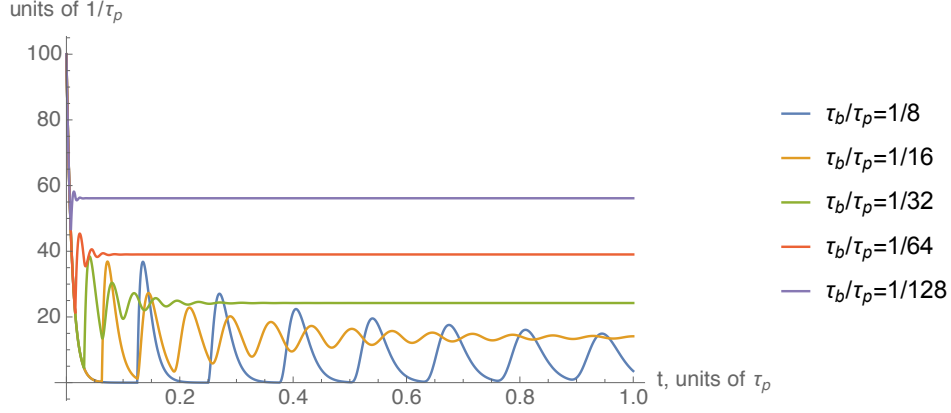


Figure S2. Ensemble-averaged output intensity  $\langle \hat{I}(t) \rangle_{\hat{\rho}} \equiv G^{(1)}(t; t)$  according to the hard-sphere ansatz (ignoring EIT filtering). Poisson-distributed input with fixed mean number of photons  $\mathcal{R}_{\text{in}} \tau_p = 100$  for different ratios of blockade time to pulse duration,  $\tau_b/\tau_p$ .

The second-order correlation function,

$$G^{(2)}(\tau_1, \tau_2; \tau_2, \tau_1) = \langle \hat{I}(\tau_1) \hat{I}(\tau_2) \rangle_{\hat{\rho}} = \langle \hat{\mathcal{E}}^\dagger(\tau_1) \hat{\mathcal{E}}^\dagger(\tau_2) \hat{\mathcal{E}}(\tau_2) \hat{\mathcal{E}}(\tau_1) \rangle_{\hat{\rho}}, \quad (\text{S9})$$

can be constructed from the diagonal elements  $G^{(1)}(\tau; \tau)$  derived in Eq. (S7) by pursuing a similar logic: As the product between the probability density of creating a polariton at time  $\tau_s + \min\{\tau_1, \tau_2\}$  conditioned on a vacant medium at  $\tau_s$  and the probability density of creating a polariton at time  $\tau_s + \max\{\tau_1, \tau_2\}$  conditioned on a polariton having been created at  $\tau_s + \min\{\tau_1, \tau_2\}$ . Importantly, the latter is independent of the event history of the time interval  $[\tau_s; \tau_s + \min\{\tau_1, \tau_2\} + \tau_b]$ . This is because the counting statistics of different time intervals of the CW input are uncorrelated and conditioning on having a Rydberg excitation created at  $\tau_s + \min\{\tau_1, \tau_2\}$  sets a boundary condition at  $t' = \tau_s + \min\{\tau_1, \tau_2\} + \tau_b$  equivalent to the initial condition at  $\tau_s$  of a vacant Rydberg medium. This argument leads to the expression:

$$G^{(2)}(\tau_1, \tau_2; \tau_2, \tau_1) = \Theta(|\tau_2 - \tau_1| - \tau_b) G^{(1)}(\min\{\tau_1, \tau_2\}; \min\{\tau_1, \tau_2\}) G^{(1)}(|\tau_2 - \tau_1| - \tau_b; |\tau_2 - \tau_1| - \tau_b). \quad (\text{S10})$$

This argument can be iterated to express the “diagonal” elements ( $\tau_i = \tau'_i$ ) of the correlation function

$$G^{(N)}(\tau_1, \dots, \tau_N; \tau'_1, \dots, \tau'_N) \equiv \langle \hat{\mathcal{E}}^\dagger(\tau_1) \hat{\mathcal{E}}^\dagger(\tau'_1) \dots \hat{\mathcal{E}}^\dagger(\tau_N) \hat{\mathcal{E}}(\tau'_N) \rangle_{\hat{\rho}} \quad (\text{S11})$$

in terms of those of  $G^{(1)}$  found in Eq. (S7). Assuming a time-ordered set  $\{\tau_1, \dots, \tau_N\}$ , Eq. (S10) generalizes to (where  $\tau_0 \equiv -\tau_b$  for convenience)

$$G^{(N)}(\tau_1, \dots, \tau_N; \tau_N, \dots, \tau_1) = \prod_{i=1}^N \theta(\tau_i - \tau_{i-1} - \tau_b) G^{(1)}(\tau_i - \tau_{i-1} - \tau_b; \tau_i - \tau_{i-1} - \tau_b). \quad (\text{S12})$$

#### IV. COMPARISON TO NUMERICAL SIMULATIONS OF 3-LEVEL MODEL FOR 2-PHOTON INPUT

To check the serialization approximation for EIT filtering used when analyzing the scheme for generating single-photon trains, we compare the results of this approximation against numerical simulations of the full set of equations of motion. The serialization approximation amounts to passing the state generated by the idealized R-R interaction [Fig. S1] through a linear EIT filter.

For the comparison, we consider square-pulse two-photon Fock-state input with (which is reasonably feasible numerically). To establish the prediction from our model, consider (for generality) an arbitrary temporal pulse shape  $h(t)$

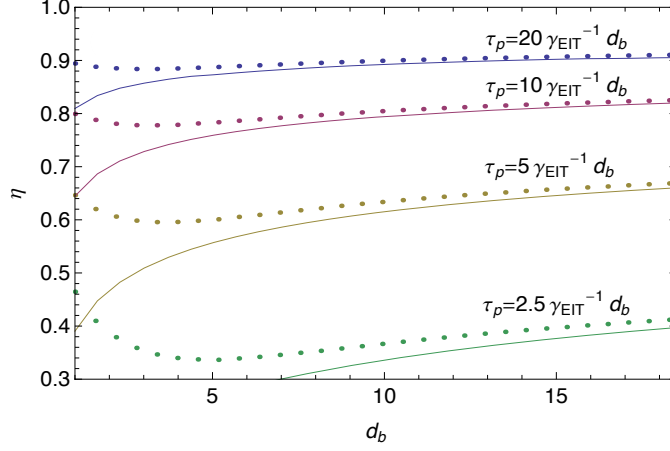


Figure S3. Transmission through a dissipative Rydberg-EIT medium. Comparison between full numerical simulation and hard-sphere ansatz with post-EIT-filtering for the propagation of a two-photon square pulse through a Rydberg medium of length  $L = r_b$ .

which is non-zero only in the time interval  $[0; \tau_{\text{end}} \geq \tau_b]$  (normalized as  $\int h^2(t) dt = 1$ ). According to the hard-sphere ansatz (ignoring single-polariton EIT decay) the density matrix when the entire pulse has entered the medium is

$$\hat{\rho}(t) = 2 \overbrace{\int_0^{\tau_{\text{end}}} d\tau_1 \int_{\max\{\tau_1 - \tau_b, 0\}}^{\tau_1} dt_1 h^2(\tau_1) h^2(t_1) |\tilde{\psi}_{\tau_1}(t)\rangle \langle \tilde{\psi}_{\tau_1}(t)|}^{\text{one scattering event}} + 2 \overbrace{\int_0^{\tau_{\text{end}} - \tau_b} dt_1 \int_{t_1 + \tau_b}^{\tau_{\text{end}}} dt_2 h^2(t_1) h^2(t_2) |\tilde{\psi}_\emptyset(t)\rangle \langle \tilde{\psi}_\emptyset(t)|}^{\text{no scattering event, } \emptyset}, \quad (\text{S13})$$

where the normalized wave functions are

$$|\tilde{\psi}_{\tau_1}(t)\rangle = \frac{-\sqrt{v_g}}{\sqrt{\int_{\max\{\tau_1 - \tau_b, 0\}}^{\tau_1} dt'_1 h^2(t'_1)}} \int_{\max\{\tau_1 - \tau_b, 0\}}^{\tau_1} dt_1 h(t_1) \hat{S}^\dagger[v_g(t - t_1)]|0\rangle, \quad (\text{S14})$$

$$|\tilde{\psi}_\emptyset(t)\rangle = \frac{v_g}{\sqrt{\int_0^{\tau_{\text{end}} - \tau_b} dt'_1 \int_{t'_1 + \tau_b}^{\tau_{\text{end}}} dt'_2 h^2(t'_1) h^2(t'_2)}} \int_0^{\tau_{\text{end}} - \tau_b} dt_1 \int_{t_1 + \tau_b}^{\tau_{\text{end}}} dt_2 h(t_1) h(t_2) \hat{S}^\dagger[v_g(t - t_1)] \hat{S}^\dagger[v_g(t - t_2)]|0\rangle. \quad (\text{S15})$$

For our special case of a square pulse we have  $h(t) = \tau_{\text{end}}^{-1/2}$ , in which case the above integrals can be straightforwardly calculated. We subject  $\hat{\rho}$  given in Eq. (S13) to linear EIT filtering corresponding to the full length  $L$  of the Rydberg medium (taking  $L = r_b$ ). We focus on the transmission of the two-photon component, i.e., the probability that neither R-R scattering nor EIT decay occurs. This amounts to filtering the second term in Eq. (S13), i.e., for square-pulse input, filtering the (unnormalized) wavefunction of the state  $(1 - \tau_b/\tau_{\text{end}})|\tilde{\psi}_\emptyset(t)\rangle$ , where  $|\tilde{\psi}_\emptyset(t)\rangle$  is given in Eq. (S15). The square norm of the filtered wavefunction is the desired transmission probability. For simplicity, we approximated the effect of a linear EIT medium by a Gaussian filter, yielding the curves presented in Fig. S3. This serialized approximation yields a pessimistic estimate, since the sharp temporal features removed by the filter are in general created somewhere in the interior of the medium thus reducing the effective optical depth of the EIT-filtering effect.

The above theoretical prediction for square-pulse 2-photon Fock-state input is compared to time-dependent numerical simulations of the pulse transmission through the medium using a three-level model for the atoms. The numerical methods are detailed in the supplementary material of Refs. [S1, S2]. The comparison is shown in Fig. S3, where we plot the transmission of the two-photon component, showing good agreement for  $d_b \gtrsim 10$ .

## V. GENERATION OF TRAINS OF SINGLE PHOTONS FROM CW INPUT

In this Appendix, we present the details behind the derivation of the requirements that the input rate  $\mathcal{R}_{\text{in}}$  has to satisfy in order to produce a regular train of single photons from CW input. Combining these requirements yield the scaling result presented as Eq. (9) in the main text.

Since  $G^{(N)}$  is simply related to  $G^{(1)}$  by Eq. (S12), we will consider the signatures of regularity in  $G^{(1)}$ . Considering the individual (unit-area) polariton peak profiles  $P_j(t - \tau_s)$  in Eq. (S7), the  $j$ 'th peak is seen to be located at

$t_j = \tau_s + j(\tau_b + 1/\mathcal{R}_{\text{in}})$  and hence the peak-to-peak separation is  $\Delta t = \tau_b + 1/\mathcal{R}_{\text{in}}$ . In the high-intensity limit, the peaks are well-separated, and we can approximate Eq. (S7) by

$$\langle \hat{I}(\tau \sim t_p - \tau_s) \rangle_{\hat{\rho}} \equiv G^{(1)}(\tau; \tau) \approx P_p(\tau), \quad (\text{S16})$$

where  $\tau \sim t_p - \tau_s$  means that  $\tau$  is in the neighborhood of the  $p$ 'th peak at  $t_p - \tau_p$  (or, more precisely, that  $p$  minimizes  $|\tau - t_p + \tau_s|$ ).

### A. Localization condition

To derive a condition for well-separated peaks, we consider the corrections to Eq. (S16), which are simply the tails of the other  $P_j$  in Eq. (S7):

$$\langle \hat{I}(\tau \sim t_p - \tau_s) \rangle_{\hat{\rho}} = P_p(\tau) + \sum_{j=1, j \neq p}^{\lceil \tau/\tau_b \rceil} P_j(\tau). \quad (\text{S17})$$

As we shall see shortly, the width of  $P_p(t)$  is sublinear in  $p$  ( $\sim \sqrt{p}$ ) and hence grows slower than  $t_p - \tau_s \propto p$ . For this reason, it is sufficient to ensure that each peak  $P_p(t)$  is well-separated from its nearest neighbors. Thus, to have a train of  $N$  well-separated photons, we must ensure that the width  $(\delta t)_N$  of the last peak  $P_N$  is much less than the peak separation,  $(\delta t)_N \ll \Delta t \approx \tau_b$  (in the high-intensity limit,  $\mathcal{R}_{\text{in}} \gg 1/\tau_b$ ). Since the  $p$ 'th peak width (HWHM) can be approximated for  $p \gg 1$  from Eq. (S6) as

$$(\delta t)_p \approx \frac{\sqrt{\ln(4)p}}{\mathcal{R}_{\text{in}}}, \quad (\text{S18})$$

this leads to the lower bound for  $\mathcal{R}_{\text{in}}$  presented in the main text (omitting the factor  $\sqrt{\ln(4)} \sim 1$  for simplicity).

### B. EIT transmittivity condition

We now present the details behind the input rate requirement imposed by the finite EIT window. Using Eq. (8) of the main text in the limit of well-separated peaks for which Eq. (S16) is applicable, we may filter the peaks individually (here assuming  $\tau_{\text{EIT}} \ll \tau_b$  and using the Gaussian EIT approximation),

$$\tilde{P}_p(\tau) \approx \int_{-\infty}^{\infty} dt_1 \int_{-\infty}^{\infty} dt_2 P_p(\min\{t_1, t_2\}) e^{-2\mathcal{R}_{\text{in}}|t_1 - t_2|} \frac{1}{2\pi\tau_{\text{EIT}}^2} e^{-\frac{(t_1 - \tau)^2}{2\tau_{\text{EIT}}^2}} e^{-\frac{(t_2 - \tau)^2}{2\tau_{\text{EIT}}^2}}. \quad (\text{S19})$$

Using Eq. (S19) we estimate the single-polariton EIT transmission  $\bar{\eta}_{\text{EIT}}$  as the integral over an individual filtered intensity peak  $\tilde{P}_p(\tau)$  [S3],

$$\bar{\eta}_{\text{EIT}} \equiv \int_{-\infty}^{\infty} d\tau \tilde{P}_p(\tau) = \exp([2\tau_{\text{EIT}}\mathcal{R}_{\text{in}}]^2) \operatorname{erfc}(2\tau_{\text{EIT}}\mathcal{R}_{\text{in}}), \quad (\text{S20})$$

which is independent of the peak number  $p$ . Expanding this in the limit  $\tau_{\text{EIT}} \ll 1/\mathcal{R}_{\text{in}}$  we find that

$$\bar{\eta}_{\text{EIT}} \approx 1 - \frac{4\mathcal{R}_{\text{in}}\tau_{\text{EIT}}}{\sqrt{\pi}} + \mathcal{O}[(\mathcal{R}_{\text{in}}\tau_{\text{EIT}})^2]. \quad (\text{S21})$$

Tolerating an EIT loss fraction of at most  $\epsilon = 1 - \bar{\eta}_{\text{EIT}}$ , we are faced with an upper bound for  $\mathcal{R}_{\text{in}}$ ,

$$\mathcal{R}_{\text{in}} \lesssim \frac{\sqrt{\pi}}{4} \frac{\epsilon}{\tau_{\text{EIT}}}, \quad (\text{S22})$$

as presented in the main text (again omitting factors of order unity for simplicity).

---

[S1] T. Peyronel, O. Firstenberg, Q.-Y. Liang, S. Hofferberth, A. V. Gorshkov, T. Pohl, M. D. Lukin, and V. Vuletic, *Nature* **488**, 57 (2012).

- [S2] M. F. Maghrebi, M. J. Gullans, P. Bienias, S. Choi, I. Martin, O. Firstenberg, M. D. Lukin, H. P. Büchler, and A. V. Gorshkov, Phys. Rev. Lett. **115**, 123601 (2015).
- [S3] The EIT loss determined here by post-filtering is found to be a factor of 2 worse than  $\bar{\eta}_{\text{EIT}}(r_b)$  as given by Eq. (S1) (comparing leading order terms in  $\mathcal{R}_{\text{in}}\tau_{\text{EIT}}$ ). We ascribe this to the additional projections that can occur when a polariton leaves the first  $r_b$  of the medium [see Appendix I and Fig. S1(d)].